Multilevel hybrid 2D strain imaging algorithm for ultrasound sector/phased arrays

Hao Chen and Tomy Varghese[a)]
Department of Medical Physics and Department of Electrical and Computer Engineering, The University of Wisconsin–Madison, Madison, Wisconsin 53706

(Received 21 October 2008; revised 13 January 2009; accepted for publication 27 March 2009; published 7 May 2009)

Two-dimensional (2D) cross-correlation algorithms are necessary to estimate local displacement vector information for strain imaging. However, most of the current two-dimensional cross-correlation algorithms were developed for linear array transducers. Although sector and phased array transducers are routinely used for clinical imaging of abdominal and cardiac applications, strain imaging for these applications has been performed using one-dimensional (1D) cross-correlation analysis. However, one-dimensional cross-correlation algorithms are unable to provide accurate and precise strain estimation along all the angular insonification directions which can range from −45° to 45° with sector and phased array transducers. In addition, since sector and phased array based images have larger separations between beam lines as the pulse propagates deeper into tissue, signal decorrelation artifacts with deformation or tissue motion are more pronounced. In this article, the authors propose a multilevel two-dimensional hybrid algorithm for ultrasound sector and phased array data that demonstrate improved tracking and estimation performance when compared to the traditional 1D cross-correlation or 2D cross-correlation based methods. Experimental results demonstrate that the signal-to-noise and contrast-to-noise ratio estimates improve significantly for smaller window lengths for the hybrid method when compared to the currently used one-dimensional or two-dimensional cross-correlation algorithms. Strain imaging results on *ex vivo* thermal lesions created in liver tissue and *in vivo* on cardiac short-axis views demonstrate the improved image quality obtained with this method. © *2009 American Association of Physicists in Medicine*. [DOI: 10.1118/1.3121426]

Key words: cross-correlation, sector, phased array, elastography, elasticity, elasticity imaging, strain, resolution, signal-to-noise ratio, contrast-to-noise ratio

I. INTRODUCTION

Elastography or techniques that image the local stiffness variations in tissue are relatively new techniques for the non-invasive evaluation of tissue mechanical properties.[1–8] In quasistatic elastography, tissue is generally deformed using a uniaxial compression, along with acquisition of pre- and post-deformation rf frames. Local strains are estimated by computing the gradient of the local displacement field along the axial direction between the pre- and post-deformation echo signal frames. Local strain images are interpreted based on the fact that stiffer tissues deform less than softer tissues under identical compressional forces, thereby providing a relative comparison of the stiffness variations in tissue.

However, much of the progress in algorithm development reported for strain imaging in the literature has been for data acquired using linear array transducers, where one-dimensional (1D),[1–5,7–10] two-dimensional (2D),[11–15] and three-dimensional (3D)[16] displacement tracking and estimation algorithms have been proposed. Algorithms for the estimation of the complete displacement vector for strain tensor estimation have also been developed.[17–19] Multiscale methods where rf data are processed in stages from a coarse to a fine scale have also been utilized.[11,13,14] In some of these multiscale approaches *B*-mode pre- and post-deformation images have been utilized as the first processing stage.[14,16] Methods to estimate tissue displacement in the presence of more general forms of tissue motion have also been implemented based on the assumption of continuity in the displacement field.[20,21] Multilevel 2D cross-correlation based methods have been utilized in situations when the displacement fields are not continuous, for example, in vascular imaging.[14] Finally, real-time implementations of strain imaging on clinical scanners have also been reported.[12]

Sector and phased array transducers are routinely used for clinical ultrasound imaging. Sector transducers are utilized extensively in abdominal, transvaginal, and transrectal applications, while phased array transducers are the de facto standard for echocardiography. Elastographic and elasticity imaging applications in these areas are rapidly gaining prominence. However, most of the current strain estimation algorithms for these geometries utilize 1D processing which possesses several limitations. Most of the previous 2D implementations of strain imaging methods have been for linear array transducers, while only 1D cross-correlation methods have been used for data acquired using sector or phased array transducers for strain imaging. One of the reasons is the difficulty in implementing 2D cross correlation for sector data since the data kernel would have a sector shape as opposed to a linear block for data. We propose a displacement and strain estimation method that utilizes multiple 1D cross-

correlation processing steps to estimate local displacements, along with 2D surface fitting on a "sector grid" or "phased array grid" to obtain subsample displacement estimates along both axial and lateral directions within the image plane.

We utilize a multilevel pyramidal technique proposed by Shi and Varghese[14] to improve computational efficiency and spatial resolution of the final strain image.[22] Processing echo signals in this manner provides high spatial resolution strain images (obtained using window lengths on the order of one to two wavelengths) without sacrificing signal-to-noise (SNR_e) or contrast-to-noise (CNR_e) ratios in the elastogram. Envelope signals (*B*-mode data) are first used to obtain a coarse estimate of the displacement, with a finer estimate of the displacement (in the neighborhood of the coarse displacement estimate) obtained by processing rf signals using window lengths on the order of one to two wavelengths.

In this paper, we present a multilevel 2D hybrid strain imaging algorithm for ultrasound sector and phased array based data. Data over the entire range of angles within the sector and phased array data format are acquired and processed (range from −45° to 45°). This algorithm addresses limitations that plague currently utilized 1D and 2D based cross-correlation methods for tracking local displacements for sector and phased array data formats. With ultrasound sector or phased array transducers, data from deeper regions in tissue are spaced further apart than those acquired from shallower regions, which lead to an increase in the lateral extent of the processing kernel for 2D methods. In addition, the relative angle between tissue deformation and the ultrasound beam direction can also change significantly leading to increased signal decorrelation artifacts.

Experimental results using uniformly elastic and single inclusion tissue-mimicking (TM) phantoms indicate that the SNR_e and CNR_e estimates obtained using the proposed hybrid algorithm are significantly higher than those obtained with the use of the currently utilized 1D or 2D cross-correlation methods. Qualitative *in vivo* experimental results for the three methods using cardiac short-axis images using a 2.5 MHz phased array transducer with rf data acquired using a GE Vingmed Vivid 7 ultrasound system (GE Medical Systems, Inc., Milwaukee, WI), are also presented.

II. MULTILEVEL HYBRID ALGORITHM FOR ULTRASOUND SECTOR/PHASED ARRAY DATA

A schematic of tissue deformation after a uniaxial compression is illustrated in Fig. 1 for sector and phased array data formats. Since each beam line has a different beam angle (either steered utilizing all the elements in the case of phased arrays or using a smaller subset of transducer elements for the sector transducers), precise location of the different features in the image can be expressed as a function of the depth along the axial direction and angle along the lateral direction. For external compression elastography, tissue is generally deformed using a quasistatic deformation along the axial direction with pre- and post-deformation rf data frames acquired. The displacement field would therefore be continuous and along the direction of compression (generally axial)

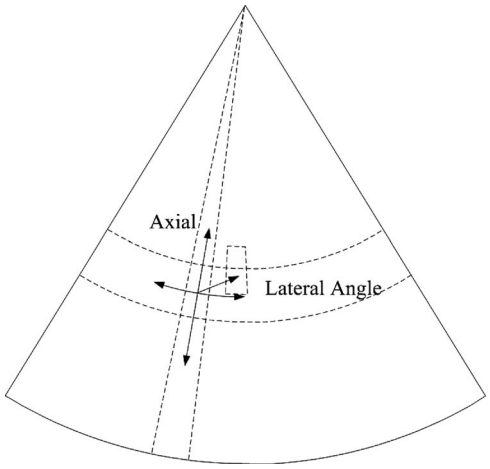

FIG. 1. Schematic of tissue deformation after an applied uniaxial compression for data acquired using a sector or phased array transducer.

with tissue expansion along the lateral and elevational directions, respectively. The displacement vector estimated from the pre- and post-deformation ultrasound data can be expressed as the displacement change along the axial direction and the lateral angle shift in the lateral direction.

Tissue deformation during strain imaging is a 3D problem, with three displacement vector components. However, for 2D imaging and tracking, we have to account for two-orthogonal displacement vectors (axial and lateral) with the displacement vector along the elevational direction ignored. For linear array transducers, in general since the directions of compression and insonification are the same, the displacement vector would contain the entire axial component of the displacement along the beam direction and the lateral component perpendicular but within the imaging plane. On the other hand for phased array and sector transducers, since the insonification direction changes for each *A* line, the displacement within the *A* line would contain partial contributions from both the axial and lateral displacement vectors, with the displacement vector estimated being along the insonification direction.

Traditional 1D cross-correlation methods have been primarily utilized for rf data acquired using a sector or phased array transducer. Local displacements are estimated along the beam propagation direction and the results displayed in a sector format. 2D processing is more complicated for these data formats, since the area and size of the 2D data block utilized for 2D cross-correlation based block matching approaches can shrink or enlarge with depth. These limitations are illustrated for data in sector or phased array formats in Fig. 1. The change in the area and/or size introduces additional estimation errors when the axial and lateral displacement vectors are directly estimated between pre- and post-deformation rf data. Assuming incompressible tissue, i.e., a Poisson ratio of 0.495, we numerically calculate the shift introduced between the pre- and post-deformation *B*-mode images for a tissue deformation of 2 mm at a 4 cm depth for both linear and phased or sector array transducers. For a beam-steered angular range of −45° to 45° with a phased

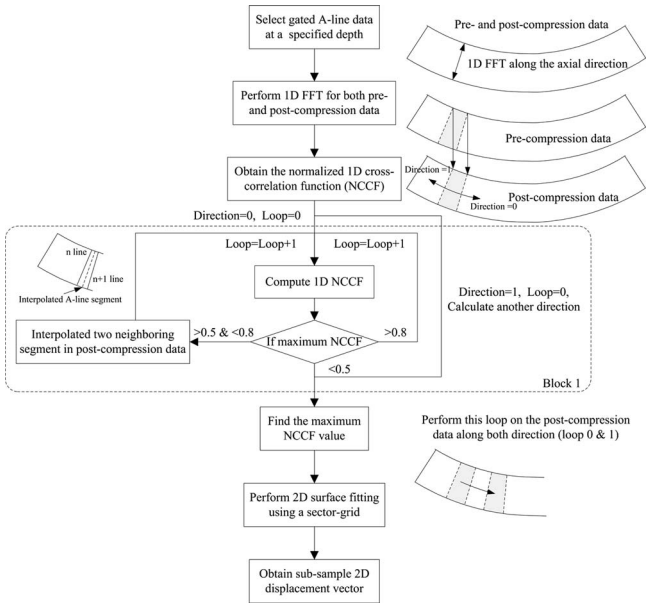

FIG. 2. Flowchart describing the multilevel hybrid 2D cross-correlation algorithm for sector or phased array data.

array and a 4 cm imaging width for the linear array transducer, with 150 scan lines each in both the *B*-mode imaging geometries, a region of interest (ROI) with dimensions of 4 mm$\times 2°$ will incur a 4.9%–5.3% change in the area over the entire angular range. The applied deformation thus introduces a 4.97 lateral beam line shift for sector or phased arrays and a 2.67 lateral beam line shift with a linear array transducer. This numerical example illustrates the difficulty with displacement tracking with sector or phased array geometries, which becomes more pronounced at increased depths due to the increased spacing between beam lines. In addition, the 2D rf data block for sector and phased array data would contain a limited number of beam lines as the pulse propagates deeper into tissue making its performance similar to 1D tracking but at a much higher computational cost.

A hybrid 2D cross-correlation algorithm is proposed in this paper to provide fast, accurate, and precise axial and lateral displacement estimations for sector and phased array data. We utilize a hierarchical search strategy using a pyramidal format to improve the computational speed of the algorithm. The initial steps utilize pre- and post-deformation envelope signals[22] obtained from rf signals to estimate coarse displacement information, since the *B*-mode data contain only amplitude information with a limited number of pixels along the axial direction when compared to the rf data. Coarse displacement estimates are then utilized to localize data segments in the final processing step performed on rf data to obtain subsample displacement estimates. The coarse displacements enable the utilization of small processing window lengths on the order of one to two wavelengths on the rf data. Figure 2 presents a flowchart describing the hybrid cross-correlation algorithm performed on the rf data. The basic steps of the hybrid 2D cross-correlation algorithm include the following:

(i) Estimate coarse displacements utilizing the 1D normalized cross-correlation function (NCCF) on the pre- and post-deformation envelope data frames. Perform a 1D FFT for the selected gated *A*-line data at a specified depth on both the pre- and post-deformation data set.
(ii) Set direction=0 and loop=0 [i.e., when direction=0, we process *A* lines on the left side of the pre-deformation *A* line and on the right side when direction=1; the parameter loop ensures that sufficient (at least one) NCCFs with high correlation coefficient values are obtained on either side of the NCCF with the largest correlation coefficient value].
(iii) Calculate the 1D NCCF for the corresponding gated *A*-line segments at specified depths on the pre-deformation data and the corresponding location on the post-deformation data based on the coarse displacement estimated and value of direction and loop.
(iv) If the maximum value of current NCCF correlation coefficient is
    (1) larger than 0.8, then loop=loop+1; repeat step (iii);
    (2) if larger than 0.5 and less than 0.8, then interpolate between the two neighboring rf segments of the post-deformation data (lateral interpolation is performed to improve the localization of the cross-correlation peak for accurate estimation of the local displacement) and recalculate the NCCF with the interpolated data, loop=loop+1; repeat step(iii);
    (3) if less than 0.5, loop$\geq$1 and direction=0, set direction=1 and loop=0 and go to step (iii);
    (4) if less than 0.5, loop$\geq$1 and direction=1, stop calculation step inside the block for the current location.
(v) Locate the peak of the cross-correlation function with maximum value over all the NCCFs in the 2D matrix.
(vi) We then utilize a 3×3 pixel region [includes the sample points (one lag value) on either side of the maximum cross-correlation peak and the NCCF on either side of the NCCF with the maximum value of the cross-correlation coefficient] to perform a 2D surface fit to obtain subsample displacement estimates along the beam direction.
(vii) This 2D surface fit accounts for the changes in beam spacing (i.e., utilizes a sector grid or phased array grid) between the *A* lines with an increase in the depth and enables the computation of a subsample 2D displacement vector.

The displacement vector obtained with the multilevel hybrid algorithm described above is therefore based on two displacement estimates: The first along the ultrasound beam direction and the second along its orthogonal direction. Both of these displacement values differ from the axial displacement obtained if the rf data were collected using linear array transducers. Figure 3 indicates the actual axial displacement along different ROIs relative to the displacement vector for the sector geometry. The axial displacement for each beam line is equal to the displacement along the beam direction

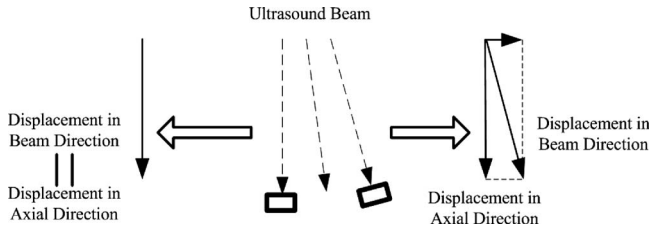

FIG. 3. Relationship between axial displacement along the insonification direction and the corresponding displacement vector.

multiplied by the cosine of the angle between the beam direction and the direction of the central ultrasound beam in the sector or phased array image, which we define as the "axial" direction. The axial strain image is then obtained by estimating the slope of the axial displacement using least squares estimation. TM phantom experiments are presented in Sec. III to evaluate the performance of the multilevel hybrid algorithm.

III. QUANTITATIVE EXPERIMENTAL ANALYSIS

III.A. Method

The strain estimation performance of the multilevel hybrid algorithm was evaluated and compared to the traditional 1D cross-correlation and 2D cross-correlation based block matching methods using both a uniformly elastic and a single inclusion TM phantom manufactured in our laboratory.[23] The uniformly elastic TM phantom has dimensions of $10\times10\times10$ cm^3. Young's modulus of the TM material was 15 kPa. The single inclusion TM phantom has dimensions of $9\times9\times9$ cm^3. This TM phantom contains a 20 mm diameter cylindrical inclusion three times stiffer than the background.[23] Young's modulus of the background material was 40 kPa while the inclusion possessed a Young's modulus of 120 kPa. All the Young's modulus measurements were performed using the ELF 3200 mechanical testing system (EnduraTEC, Minnetonka, MN) in our laboratory.

The TM phantom was immersed in a safflower oil bath and scanned using a real-time clinical Antares Ultrasound Scanner (Siemens Medical Solutions USA, Inc., Ultrasound Division, Issaquah, WA) using a phased array transducer (PH 4-1) with a center frequency of 2.22 MHz and 70% bandwidth. The phased array transducer provided 336 *A* lines over a beam-steered angular range of −45.1° to 45.1° within a single rf data frame. A single transmit focus was set at a depth of 70 mm in the uniformly elastic phantom and at a depth of 40 mm in the inclusion phantom with dynamic focusing on receive. A compression plate with a rectangular slot to match the transducer face was mounted within a linear translation stage driven by a stepper motor controlled by a computer. The compression plate was larger than the phantom surface and provides a uniform deformation of the phantom. Echo signals were acquired originating from the top of the phantom to a depth of 10 cm for the uniformly elastic TM phantom and 9 cm for the TM inclusion phantom before and after an axial compression of 0.5%—2% of the phantom height. An initial pre-compression of 3% was applied to ensure proper contact between the compression plate and the phantom. The placement of the phantom in the safflower oil bath provides a thin film of oil on the top and bottom surfaces of the phantom to ensure slip boundary conditions.

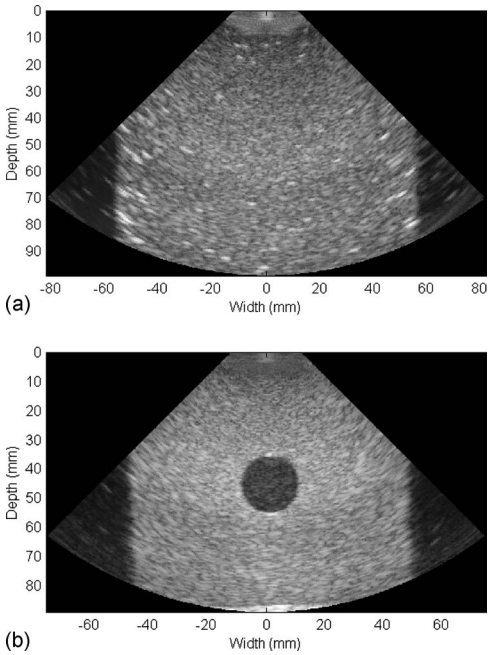

FIG. 4. *B*-mode image of the (a) uniformly elastic TM phantom and (b) single inclusion TM phantom.

The entire experiment was repeated ten times at different locations on the phantom to obtain independent rf data realizations. Ultrasound rf signals were digitized at a sampling rate of 40 MHz and stored in a personal computer for off-line analysis. Figure 4 presents the *B*-mode image of the uniformly elastic TM phantom (a) and the single inclusion TM phantom (b).

Pre- and post-compression rf echo signals were analyzed using the multilevel hybrid method, the traditional 1D cross-correlation method, and the 2D cross-correlation block matching method. For the 1D cross-correlation analysis method, we utilize only two steps since the first step that utilizes *B*-mode data does not provide any significant improvement with the subsequent two stages with the rf data. However, both the conventional 2D method and the hybrid technique proposed in this paper utilize three processing steps. The first correlation step for the multilevel hybrid and 2D cross-correlation methods uses 50% overlapped kernels with an axial dimension of 24 wavelengths and includes 11 beam lines. The second step of the multilevel hybrid method uses 75% overlapped kernels with 12 wavelengths and seven *A* lines. The third step of the multilevel hybrid method uses 75% overlapped 2D kernels with four wavelengths and five beam lines. The 2D cross-correlation based method uses the exact same parameters as the three stages of the multilevel hybrid method (where the *A*-line range here indicates the search range for displacement tracking). The first correlation step of the traditional 1D cross-correlation method uses 50%

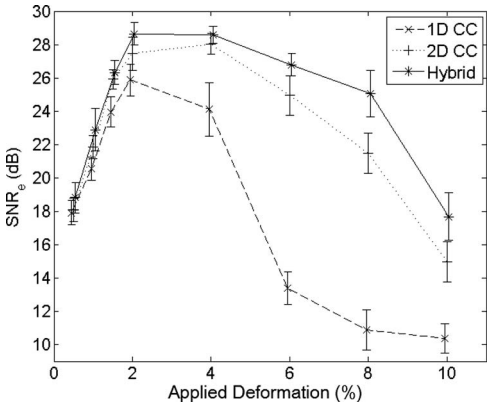

FIG. 5. Plots of the SNR$_e$ versus applied compression for the traditional 1D cross-correlation method, 2D cross-correlation block matching method, and multilevel 2D hybrid method.

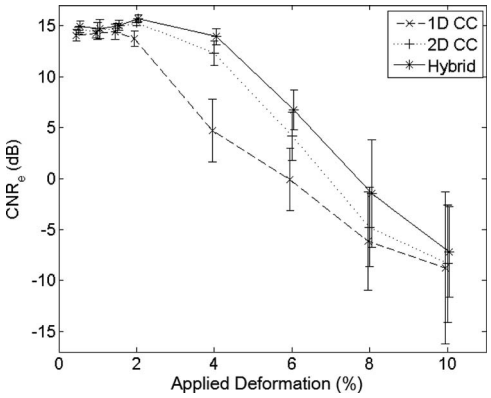

FIG. 6. Plots of the CNR$_e$ versus applied compression for the traditional 1D cross-correlation method, 2D cross-correlation block matching method, and multilevel 2D hybrid method.

overlapped window with 24 wavelengths. The second step of the traditional cross-correlation method uses 75% overlapped window with four wavelengths.

All the strain imaging algorithms were evaluated under a MATLAB environment (The MathWorks, Natick, MA). MATLAB routines were run on a Dell Dimension 3000 with a Pentium 3 GHz CPU, 1 Gbyte of RAM, and Microsoft Windows XP Professional with service pack 2. The 1D traditional cross-correlation method using the two-step method[22] requires 120 s (mean value) to obtain a single frame of the strain image. The 2D cross-correlation method requires 610 s (mean value) to obtain a strain image frame. The computational load with the multilevel hybrid method is between the previously described methods at 300 s (mean value) to process and obtain a single frame of the strain image.

IV. RESULTS

The mean and variance of the strain estimates used to calculate the SNR$_e$ were obtained using the uniformly elastic phantom while the single inclusion phantom was utilized to obtain CNR$_e$ comparisons. Definitions of the SNR$_e$ and CNR$_e$ terms are presented in the Appendix. Quantitative estimates of the mean and standard deviation of the strain estimates obtained using the multilevel hybrid method are compared to the traditional 1D cross-correlation method and 2D cross-correlation method. Strain estimates obtained from a ROI between a depth of 30 and 50 mm around the transmit focus of the transducer were utilized. An applied deformation of 0.5%—2% of the phantom height was used in this analysis.

Figure 5 presents the variation in the SNR$_e$ obtained from the axial strain image of the uniformly elastic phantom. As the applied deformation increases from 0.5% to 2%, the SNR$_e$ values indicate a decreasing trend with the traditional 1D cross-correlation method. Larger applied deformations increase the lateral movement of the scatterers, thereby increasing lateral decorrelation artifacts. On the other hand, SNR$_e$ values obtained using the 2D methods do not decrease with an increase in the applied deformation from 0.5% to 2%, since the 2D cross-correlation methods efficiently track the lateral displacement when compared to the 1D methods. However, all the methods present similar performances when the applied deformation is small (0.5%). The multilevel hybrid method provides SNR$_e$ values that are about 2 dB higher than 2D cross-correlation block matching method and about 3 dB higher than 1D cross-correlation method when the applied compression is 1%. In addition, the multilevel hybrid method is two times faster than the corresponding 2D cross-correlation method.

The inclusion region for the phantom utilized for the CNR$_e$ comparisons is located between depths of 4 and 5 cm and for lateral angles ranging from −5.5° to 5.5° obtained from the *B*-mode image of the inclusion phantoms. Two regions selected for the background are located on both sides of the inclusion and at the same depth as the ROI within the inclusion region. The background region on the left is located at lateral angles ranging from −19.5° to −14.0°, while the background region on the right is located at angles from 14.0° to 19.5°, respectively. Each of the background regions includes a lateral angular region of 5.5°, such that the total areas of the inclusion region and background region remain the same. This scheme enables repeatable selection of the same region across strain images, and the user only has to select the center of the inclusion.

Figure 6 presents a comparison of the CNR$_e$ variation obtained versus the applied deformation for the three methods. Note that the CNR$_e$ values obtained with the multilevel hybrid method is larger than that obtained with either the 2D cross-correlation method or the 1D cross-correlation method over the entire range of applied deformations. When the applied compression is increased from 0.5% to 1%, the CNR$_e$ value obtained also increases for all the methods. The CNR$_e$ with the multilevel hybrid method and 2D cross-correlation method remains constant when the applied compression increases from 1% to 2%, while the CNR$_e$ with the traditional cross-correlation decreases due to increased lateral decorrelation. The multilevel hybrid method provides CNR$_e$ values that are about 0.5 dB better than that obtained with the 2D

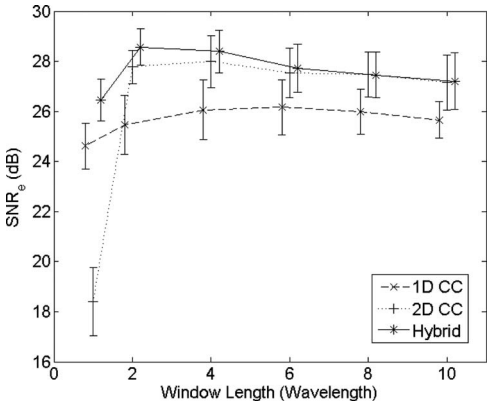

FIG. 7. Plots of the SNR$_e$ versus the axial dimensions of kernel for the last processing step for the traditional 1D cross-correlation method, 2D cross-correlation block matching method, and multilevel 2D hybrid method. The applied compression was 2% of the phantom height.

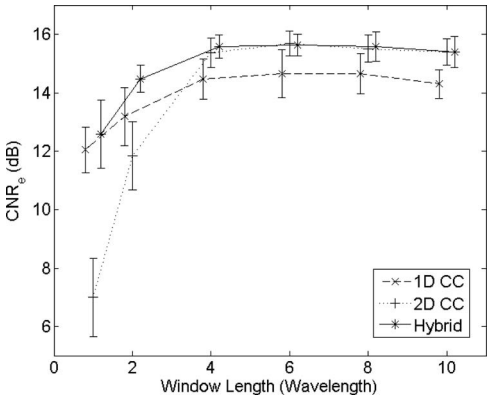

FIG. 8. Plots of the CNR$_e$ versus the dimension of kernel along the axial direction for the last processing step for the traditional 1D cross-correlation method, 2D cross-correlation block matching method, and the multilevel 2D hybrid method. The applied compression was 2% of the phantom height.

cross-correlation method for an applied compression of 1% and about 1.5 dB better than 1D cross-correlation method for an applied compression of 2%.

IV.A. Performance relative to kernel dimensions

Pre- and post-compression rf data for the TM phantom before and after an axial compression of 2% of the phantom height was utilized to evaluate the performance of the three methods with a decrease in the processing kernel dimensions or improvement in the spatial resolution in the strain image. The first and second processing steps of the multilevel method were the same as described earlier, while the kernel dimensions in the third step uses 75% overlapped 2D kernels with one, two, four, six, eight, and ten wavelengths along the axial dimension and five *A* lines along the lateral directions. In a similar manner, the 2D cross-correlation based block matching method was also evaluated using 75% overlapped 2D window with one, two, four, six, eight, and ten wavelengths and five beam lines, while the second step of the traditional cross-correlation method uses 75% overlapped window with one, two, four, six, eight, and ten wavelengths, respectively.

Figure 7 presents a comparison of the SNR$_e$ variation versus the window length of the last step for the three methods, while the corresponding variation in the CNR$_e$ is illustrated in Fig. 8. Note that the SNR$_e$ and CNR$_e$ values obtained with the multilevel hybrid method is larger than that obtained with either the 2D cross-correlation block matching method or the 1D cross-correlation method over all the axial window dimensions presented. The multilevel hybrid method provides SNR$_e$ improvements that are about 2 dB better than the 1D cross-correlation method and CNR$_e$ about 1 dB better than 1D cross-correlation method for almost all the window lengths used. The multilevel hybrid method provides better SNR$_e$ and CNR$_e$ than the 2D cross-correlation block matching method for window lengths less than four wavelengths and similar performance for window lengths larger than four wavelengths.

V. *EX VIVO* STRAIN IMAGING RESULTS OF THERMAL LESION IN LIVER TISSUE

V.A. Data acquisition and processing

Sector data were acquired from a thermally ablated lesion created in *ex vivo* liver tissue utilizing a Antares Ultrasound system, equipped with a C7F2 4D wobbler transducer.[24] The Siemens C7F2 fourSight 4D transducer is a "wobbling" 1D curved linear array and was operated at a 4.4 MHz center frequency. The array has 192 elements and the curvature allows a maximum sector angle of about 80°. The maximum sweeping (wobbling) angle of the array is 75° (perpendicular to the image plane). A single transmit focus was applied, at a depth of 4 cm, and dynamic focusing was used on receive. This system provides rf data for an 8 cm depth at a 40 MHz sampling rate. Pre- and post-deformation rf data were obtained in a "stepped" mode, where the array is first moved to the angular position as read from a look-up table and a data acquisition frame sequence is triggered after movement of the array has ceased.[24]

Figure 9(a) presents a *B*-mode image of the *ex vivo* liver with the thermal lesion. The multilevel hybrid technique utilizes *B*-mode image data in the first processing step which utilizes 50% overlapped gated windows with a 20 wavelength window length along the beam direction and 11 *A* lines along the azimuthal direction. For the second processing step a 75% overlapped eight wavelength window length and seven beam lines along the azimuthal direction are used. The final step (third correlation step) uses rf data with 75% overlapped gated windows and a four wavelength window length and five beam lines along the azimuthal direction.

V.B. Strain image of *ex vivo* thermal lesion in the liver

Figure 9(b) depicts a strain image obtained with the 2D multilevel hybrid method, while Fig. 9(c) presents the corresponding results obtained using a 1D cross-correlation method and Fig. 9(d) utilizing a 2D block matching method. Observe from Fig. 9 that the strain images obtained using the

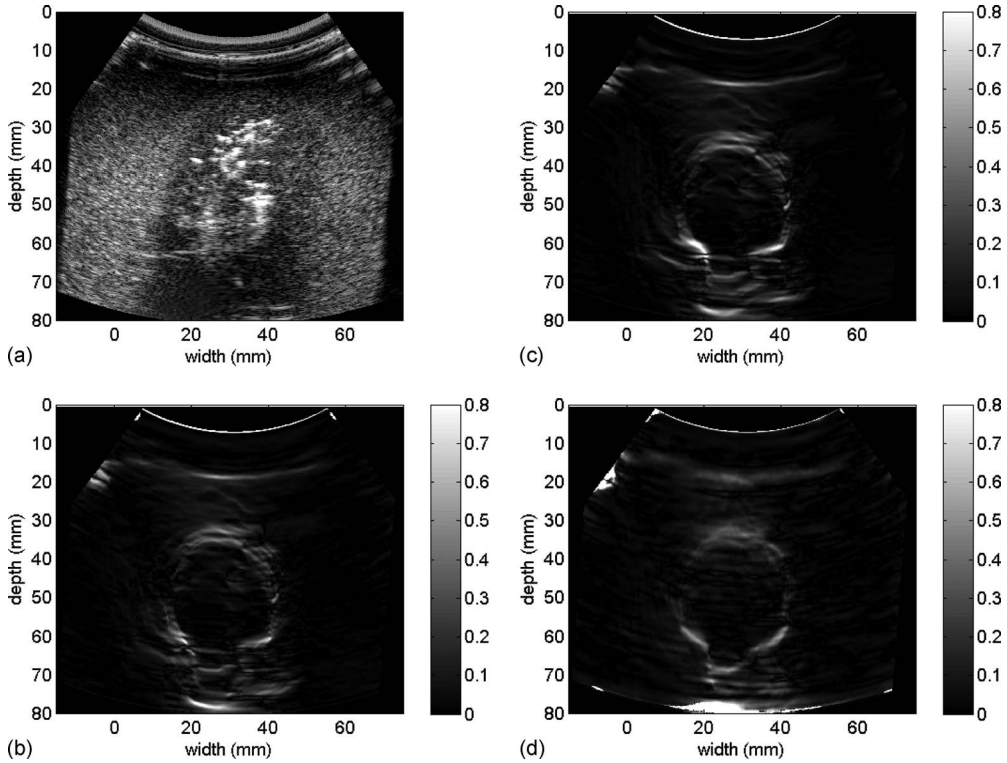

FIG. 9. Qualitative *ex vivo* depiction of a thermal lesion created in liver tissue. (a) *B*-mode image, axial strain image (b) for the 2D multilevel hybrid method, along with axial strain images using a (c) 1D cross-correlation method and (d) 2D block matching method.

2D multilevel hybrid techniques [Fig. 9(b)] provide the sharpest boundary and high SNR_e and CNR_e regions inside the thermal lesion and in the background tissue. The improved boundary delineation obtained with the 2D multilevel hybrid technique provides significantly improved spatial resolution in the strain image when compared with both the 1D cross-correlation and 2D cross-correlation methods. Note the increased blurring in the strain image obtained with the 1D cross-correlation and 2D cross-correlation method in Figs. 9(c) and 9(d), respectively. We have previously demonstrated close correlations between strain and pathology images for thermally ablated regions.[25–27] Figure 9 demonstrates the improved strain images obtained using the multilevel hybrid algorithm for data in a sector format.

VI. COMPARISON OF *IN VIVO* CARDIAC STRAIN IMAGES

VI.A. Data acquisition

Healthy volunteers were scanned using a GE Vingmed Vivid 7 ultrasound system (GE Medical Systems, Inc., Milwaukee, WI) using a 2.5 MHz phased array transducer having an approximately 60% bandwidth. The transducer provides 114 *A* lines in a single rf data frame over a 75° sector angle. A single transmit focus was applied, set at a depth around 10 cm, and dynamic focusing used on receive. This system provides rf data for a 15 cm depth at a 20 MHz sampling rate and at a frame rate of 34.1 frames per second (FPS). Each data set contains 201 frames rf data and was stored in a personal computer for off-line analysis.

For the multilevel hybrid technique, *B*-mode image data, shown in Fig. 10(a), are used in the first processing step, which utilizes 50% overlapped gated windows with a 28 wavelength window length along the beam direction and seven *A* lines along the azimuthal direction. The second correlation step uses rf data using 75% overlapped gated windows with a 12 wavelength window length and five beam lines along the azimuthal direction. The positions of the gated segments in the rf data in the frame sequence were registered using displacement information obtained from the *B*-mode image data prior to tracking the displacements on the corresponding rf data set. Figure 10(b) shows a single frame of the strain obtained with the 2D multilevel hybrid method, while Fig. 10(c) presents the corresponding results for the 1D cross-correlation method and Fig. 10(d) for the 2D cross-correlation method.

Observe from Fig. 10 that the strain images obtained using the 2D multilevel hybrid techniques [Fig. 10(b)] provide low noise and smoother images with the highest SNR_e and CNR_e values. On the other hand strain images obtained using both the 1D cross-correlation and 2D cross-correlation methods provide images with increased noise artifacts.

Note that large deformations may occur under clinical imaging conditions due to patient motion or physiological causes, for example, for cardiac imaging deformations during systole can be quite large.[28] Therefore for accurate displacement tracking of the cardiac wall motion, high frame rates are essential. For cases when the frame rates are not sufficiently high, tissue deformation would be large between

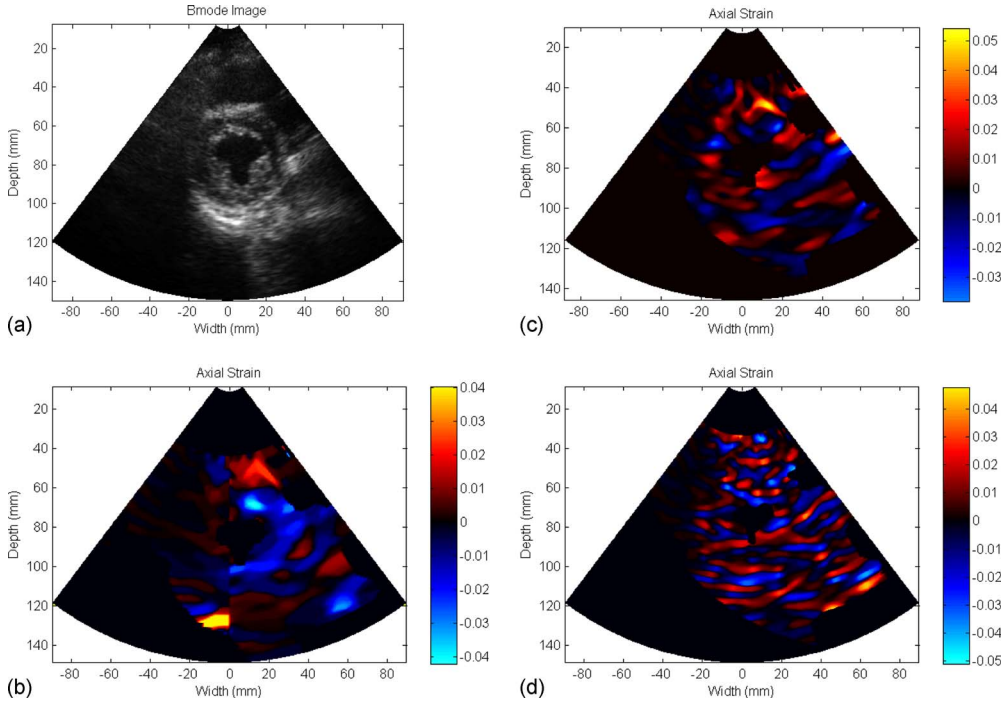

FIG. 10. (a) Qualitative *in vivo* cardiac short-axis *B*-mode echocardiographic image, along with axial strain image using the (b) 2D multilevel hybrid method, (c) with a 1D cross-correlation method, and (d) for the 2D block matching method.

sequential rf frames.[28] In this paper, we also demonstrate the ability of the hybrid algorithm to track large applied deformations (see Figs. 5 and 6); however, a concomitant decrease in the SNR_e and CNR_e is also present due to increased signal decorrelation with deformation.

VII. DISCUSSION AND CONCLUSIONS

Sector transducers are utilized extensively in abdominal, transvaginal, and transrectal applications, while phased arrays are the de facto standard for echocardiography. Elastographic and elasticity imaging applications in these areas are rapidly gaining prominence. However, most of the current strain estimation algorithms for these geometries utilize 1D processing which has several limitations. We present a fast and robust multilevel hybrid 2D cross-correlation algorithm for ultrasound sector and phased array data that provide accurate and precise (from the error bar height, indicating repeatability of the estimated strain) strain estimation.

We utilize a hierarchical multilevel search strategy using a pyramidal format to improve the computational speed of the algorithm. The initial step utilizes pre- and post-compression envelope signals obtained from the rf signals to estimate coarse displacement estimates. Coarse displacement estimates are then utilized to localize data segments for the final processing step performed on rf data to obtain subsample displacement estimates using window lengths on the order of one to two wavelengths. We estimate the normalized 1D cross-correlation function using a gated rf data segment on the pre-deformation data and the corresponding segment on the post-deformation data. In addition, several NCCFs are obtained using the same pre-deformation data segment and additional data segments in the post-deformation data on either side of the original pre-deformation data segment. The NCCFs are stacked together and the maximum value within this matrix determines the location of the displacement. Subsample displacement estimates are obtained by performing a 2D surface fit utilizing a sector-grid or phased array grid coordinates. Strain images are obtained through slope estimation using least squares estimation.

Tissue-mimicking phantom experiments were utilized to evaluate the performance of the multilevel hybrid algorithm in terms of the SNR_e and CNR_e properties and compared with the two-step 1D cross-correlation and 2D cross-correlation methods. The results indicate that the hybrid method provides improved SNR_e and CNR_e in the TM phantom when compared to the other two methods. The performance of 1D cross correlation reduces with increased applied compression and at deeper depths in the phantom. The multilevel hybrid method provides precise estimation of the displacement using window lengths on the order of a wavelength while preserving the noise properties of the strain image. The hybrid method also provides robust and faster estimation of the displacement and is about two times faster than the 2D cross-correlation method.

Both the *ex vivo* thermal lesion results in the liver and the *in vivo* cardiac data demonstrate the improved strain estimation performance of the 2D hybrid method when compared to the 1D cross-correlation and 2D cross-correlation methods. The hybrid method also provides sharper boundaries, demonstrating the improved spatial resolution along with smoother strain distributions within the thermal lesion and in the background (higher SNR_e and CNR_e).

ACKNOWLEDGMENTS

This work was funded in part by NIH Grant No. R01 CA112192-02 and funds from the Graduate School, UW-Madison provided by the Wisconsin Alumni Research Foundation.

APPENDIX: STRAIN IMAGING QUALITY PARAMETERS

I. Signal-to-noise ratio

The signal-to-noise ratio (SNR_e) in elastography is a quantity used to describe the noise properties of the strain image. The SNR_e is defined as[29,30]

$$\mathrm{SNR}_e = \frac{m_s}{\sigma_s}, \tag{A1}$$

where m_s and σ_s denote the mean and the standard deviation of the estimated strain, respectively.

II. Contrast-to-noise ratio

The contrast to-noise ratio (CNR_e) is a quantity that determines the detectability of lesions.[31] The CNR_e for elastography is defined as follows:[31]

$$\mathrm{CNR}_e = \frac{2(e_B - e_I)^2}{\sigma_{eB}^2 + \sigma_{eI}^2}, \tag{A2}$$

where e_B and e_I represent mean strains in the background and inclusion while σ_{eB} and σ_{eI} represent standard deviations of background and inclusion, respectively.

[a]Author to whom correspondence should be addressed. Electronic mail: tvarghese@wisc.edu; Telephone (608)-265-8797; Fax: (608)-262-2413.

[1]J. Ophir, I. Cespedes, H. Ponnekanti, Y. Yazdi, and X. Li, "Elastography: A quantitative method for imaging the elasticity of biological tissues," Ultrason. Imaging **13**, 111–134 (1991).
[2]I. Cespedes, J. Ophir, H. Ponnekanti, and N. Maklad, "Elastography: Elasticity imaging using ultrasound with application to muscle and breast in vivo," Ultrason. Imaging **15**, 73–88 (1993).
[3]M. Bilgen and M. F. Insana, "Deformation models and correlation analysis in elastography," J. Acoust. Soc. Am. **99**, 3212–3224 (1996).
[4]E. J. Chen, R. S. Adler, P. L. Carson, W. K. Jenkins, and W. D. O'Brien, Jr., "Ultrasound tissue displacement imaging with application to breast cancer," Ultrasound Med. Biol. **21**, 1153–1162 (1995).
[5]H. E. Talhami, L. S. Wilson, and M. L. Neale, "Spectral tissue strain: A new technique for imaging tissue strain using intravascular ultrasound," Ultrasound Med. Biol. **20**, 759–772 (1994).
[6]Y. Zhu and T. J. Hall, "A modified block matching method for real-time freehand strain imaging," Ultrason. Imaging **24**, 161–176 (2002).
[7]A. Pesavento, C. Perrey, M. Krueger, and H. Ermert, "A time-efficient and accurate strain estimation concept for ultrasonic elastography using iterative phase zero estimation," IEEE Trans. Ultrason. Ferroelectr. Freq. Control **46**, 1057–1067 (1999).
[8]M. O'Donnell, A. R. Skovoroda, B. M. Shapo, and S. Y. Emelianov, "Internal displacement and strain imaging using ultrasonic speckle tracking," IEEE Trans. Ultrason. Ferroelectr. Freq. Control **41**, 314–325 (1994).
[9]S. Srinivasan, J. Ophir, and S. K. Alam, "Elastographic imaging using staggered strain estimates," Ultrason. Imaging **24**, 229–245 (2002).
[10]T. Varghese, M. Bilgen, and J. Ophir, "Multiresolution imaging in elastography," IEEE Trans. Ultrason. Ferroelectr. Freq. Control **45**, 65–75 (1998).
[11]P. Chaturvedi, M. F. Insana, and T. J. Hall, "2-D companding for noise reduction in strain imaging," IEEE Trans. Ultrason. Ferroelectr. Freq. Control **45**, 179–191 (1998).
[12]Y. Zhu and T. J. Hall, "A modified block matching method for real-time freehand strain imaging," Ultrason. Imaging **24**, 161–176 (2002).
[13]C. Pellot-Barakat, F. Frouin, M. F. Insana, and A. Herment, "Ultrasound elastography based on multiscale estimations of regularized displacement fields," IEEE Trans. Med. Imaging **23**, 153–163 (2004).
[14]H. Shi and T. Varghese, "Two-dimensional multi-level strain estimation for discontinuous tissue," Phys. Med. Biol. **52**, 389–401 (2007).
[15]J. Jiang and T. J. Hall, "A parallelizable real-time motion tracking algorithm with applications to ultrasonic strain imaging," Phys. Med. Biol. **52**, 3773–3790 (2007).
[16]A. V. Patil, C. D. Garson, and J. A. Hossack, "3D prostate elastography: Algorithm, simulations and experiments," Phys. Med. Biol. **52**, 3643–3663 (2007).
[17]E. Konofagou and J. Ophir, "A new elastographic method for estimation and imaging of lateral displacements, lateral strains, corrected axial strains and Poisson's ratios in tissues," Ultrasound Med. Biol. **24**, 1183–1199 (1998).
[18]M. Rao, Q. Chen, H. Shi, T. Varghese, E. L. Madsen, J. A. Zagzebski, and L. S. Wilson, "Normal and shear strain estimation using beam steering on linear-array transducers," Ultrasound Med. Biol. **33**, 57–66 (2007).
[19]U. Techavipoo, Q. Chen, T. Varghese, and J. A. Zagzebski, "Estimation of displacement vectors and strain tensors in elastography using angular insonifications," IEEE Trans. Med. Imaging **23**, 1479–1489 (2004).
[20]Y. Zhu, P. Chaturvedi, and M. F. Insana, "Strain imaging with a deformable mesh," Ultrason. Imaging **21**, 127–146 (1999).
[21]R. L. Maurice, J. Ohayon, Y. Fretigny, M. Bertrand, G. Soulez, and G. Cloutier, "Noninvasive vascular elastography: Theoretical framework," IEEE Trans. Med. Imaging **23**, 164–180 (2004).
[22]H. Chen, H. Shi, and T. Varghese, "Improvement of elastographic displacement estimation using a two-step cross-correlation method," Ultrasound Med. Biol. **33**, 48–56 (2007).
[23]E. L. Madsen, G. R. Frank, T. A. Krouskop, T. Varghese, F. Kallel, and J. Ophir, "Tissue-mimicking oil-in-gelatin emulsions for use in heterogeneous elastography phantoms," Ultrason. Imaging **25**, 17–38 (2003).
[24]S. Bharat, T. Fisher, T. Varghese, T. Hall, J. Jiang, E. Madsen, J. Zagzebski, and F. J. Lee, "Three-dimensional electrode displacement elastography using the Siemens C7F2 fourSight four-dimensional ultrasound transducer," Ultrasound Med. Biol. **34**, 1307–1316 (2008).
[25]T. Varghese, U. Techavipoo, W. Liu, J. Zagzebski, Q. Chen, G. Frank, and F. J. Lee, "Elastographic measurement of the area and volume of thermal lesions resulting from radiofrequency ablation: Pathologic correlation," AJR, Am. J. Roentgenol. **181**, 701–707 (2003).
[26]W. Liu, U. Techavipoo, T. Varghese, J. Zagzebski, Q. Chen, and F. J. Lee, "Elastographic versus x-ray CT imaging of radio frequency ablation coagulations: An in vitro study," Med. Phys. **31**, 1322–1332 (2004).
[27]G. Pareek, E. Wilkinson, S. Bharat, T. Varghese, P. Laeseke, F. J. Lee, T. Warner, J. Zagzebski, and S. Nakada, "Elastographic measurements of in-vivo radiofrequency ablation lesions of the kidney," J. Endourol **20**, 959–964 (2006).
[28]H. Chen, T. Varghese, P. S. Rahko, and J. A. Zagzebski, "Ultrasound frame rate requirements for cardiac elastography: Experimental and in-vivo results," Ultrasonics **49**, 98–111 (2009).
[29]I. Cespedes and J. Ophir, "Reduction of image noise in elastography," Ultrason. Imaging **15**, 89–102 (1993).
[30]T. Varghese and J. Ophir, "A theoretical framework for performance characterization of elastography: The strain filter," IEEE Trans. Ultrason. Ferroelectr. Freq. Control **44**, 164–172 (1997).
[31]T. Varghese and J. Ophir, "An analysis of elastographic contrast-to-noise ratio," Ultrasound Med. Biol. **24**, 915–924 (1998).